Do Main Chain Hydrogen Bonds Create Dominant Electron Transfer Pathways? An Investigation in Designed Proteins†

Yongjian Zheng,‡ Martin A. Case,‡ James F. Wishart,§ and George L. McLendon*,‡

The Department of Chemistry, Princeton University, Princeton, New Jersey 08544-1009, and Brookhaven National Laboratory, Upton, New York 11973-5000

Received: September 27, 2002

We have investigated the contribution of main chain hydrogen bond (H-bond) pathways to the tunneling matrix elements which control electron transfer (ET) rates across an α-helical protein matrix. The paradigm system for these investigations is a metal ion-assembled parallel three-helix bundle protein that contains a ruthenium(II) tris(bipyridyl) electron donor and a ruthenium(III) pentammine electron acceptor separated by a direct metal to metal distance of ca. 19 Å, requiring tunneling through 15 Å of α-helical peptide. The putative ET pathway was modulated by a synthetic strategy in which specific main chain amide moieties along an α-helix were replaced by ester linkages that cannot form equivalent H-bonds. A simple pathway analysis implies a role for such H-bonds in facilitating electron transfer. Within the accuracy of the computational predictions, specific H-bonded pathway models do not predict the differences in the measured ET rates between the parent construct and the different H-bond deletion variants.

Introduction

Electron-transfer reactions within and between proteins are ubiquitous in biology.[1−3] Given this centrality it is interesting to explore the role played by the protein in "tuning" electron transfer rates. Two (limiting) positions have been suggested. The first suggests that the protein is a "generic organic matrix" in which the coupling between an electron donor (D) and acceptor (A) depends primarily on the D−A distance.[4−8] This approach provides an algorithm for predicting electron-transfer rates as a function of D−A distance. The alternative posits that specific "pathways" exist in proteins, composed of covalent connections, H-bond connections, and nonbonded connections.[9−15] In this model accurate rate predictions depend on identifying the dominant composite "bond-equivalent" pathways, rather than simply specifying the distance.

In practice, the distinction between distance models and pathway models depends on the relative weighting factors assigned to each type of connection. If coupling via a covalent connection were identical to that via a nonbonded connection, then the pathway model could reduce to the simple distance model.[16,17] Thus a critical parameter in defining and applying these models is the relative efficiency of hydrogen bonds in promoting electronic coupling.[18−21] In the electronic coupling model developed by Beratan and Onuchic,[10−15] a hydrogen bond is much more effective than noncovalent "through space" tunneling. It has, however, proven very difficult to experimentally test the role of H-bonds in proteins, although the role of H-bond mediated coupling has been studied in small molecules.[22,23] Conventional mutagenesis of natural proteins often results in subtle structural rearrangements, and main chain H-bonds cannot be replaced by normal techniques of site-directed mutagenesis.

We here report detailed studies of de novo designed redox proteins tailored to address these issues. The system of interest is a metal ion assembled three-helix bundle protein, as shown in Figure 1.

A rationale for the amino acid sequences of the three helices has been detailed elsewhere,[24,25] and the structural robustness of such assemblies is well documented.[24−28] The electron donor is an N-terminal ruthenium(II) tris(bipyridyl) derivative that is built into the structure in the assembly process.[27,28] The electron acceptor is a ruthenium(III) pentammine bound to the imidazole N_ϵ of a histidine residue nine amino acids along one of the three α-helices. Using a modified solid-phase peptide synthesis (SPPS) strategy, specific amide bonds in the intervening peptide sequence were replaced by ester homologues. Though amide protons at the *i*th position of an α-helix form main chain H-bonds to carbonyl oxygen atoms at the (*i*+4)th position, the ester homologues are incapable of such bonding. Comparison of the rates of electron transfer in the "wild type" and H-bond deleted variants allows an explicit assessment of the contribution of main chain H-bonds to electron transfer for the first time.

Experimental Section

For H-bond deletion studies, the following peptides were synthesized:

bpy-GELAQKLEQALQKLEQALQK-amide	αP
bpy-GELAQKLQHALQKLEQALQK-amide	αP9H
bpy-GELAQKLφ(QH)ALQKLEQALQK-amide	αP9Hφ(QH)
bpy-GELAQKφ(LQ)HALQKLEQALQK-amide	αP9Hφ(LQ)
bpy-GELAQφ(KL)QHALQKLEQALQK-amide	αP9Hφ(KL)

φ(AB) denotes a backbone ester linkage between residues A and B. Peptides were synthesized via a modified Fmoc SPPS protocol, as described in the Supporting Information.

The stepwise ruthenium(II)-assisted assembly of the heterotrimers $[Ru(\alpha P)_2(\alpha P^*)]^{2+}$ (where αP* is any of the variants listed above) has been described elsewhere,[27−29] as has the subsequent derivatization of the unique histidine residue with the $[Ru(NH_3)_5]^{3+}$electron acceptor.[27,28]

† Part of the special issue "Arnim Henglein Festschrift".

* Corresponding author. Telephone: 609-258-6808. Fax: 609-258-6746. E-mail: glm@princeton.edu.

‡ The Department of Chemistry, Princeton University.

§ Brookhaven National Laboratory.

10.1021/jp027092u CCC: $25.00
Published on Web 05/21/2003

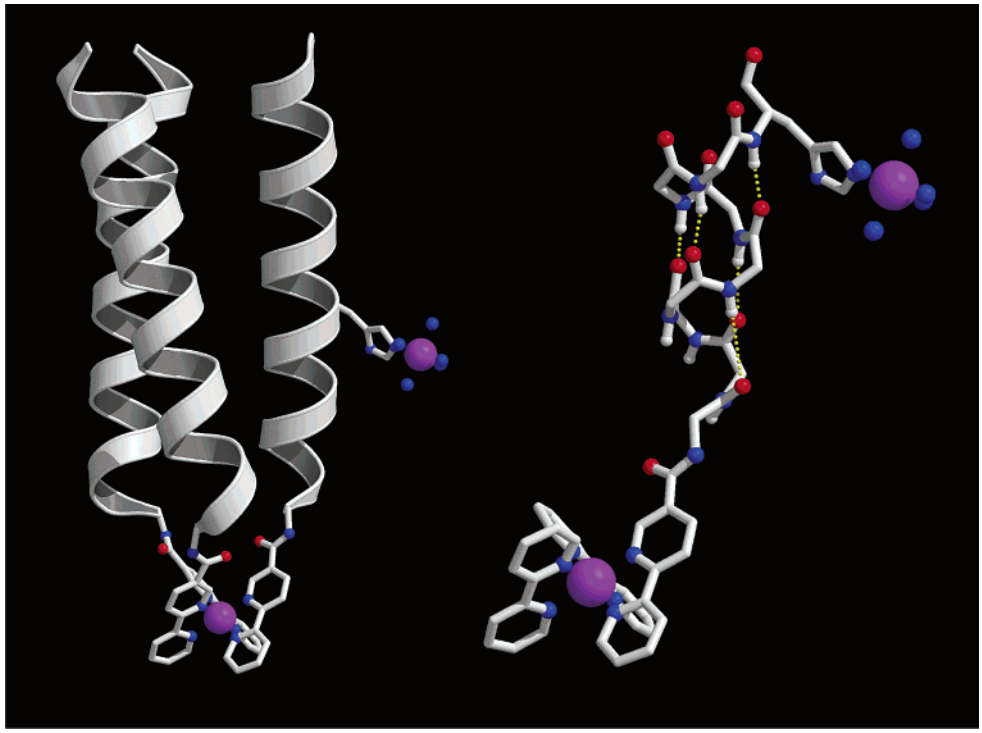

Figure 1. Left: schematic illustration of the parallel three-helix bundle used in these studies. The $[Ru(bpy)_3]^{2+}$ electron donor and the $[Ru(NH_3)_5(his)]^{3+}$ electron acceptor are shown explicitly. The donor−acceptor distance is ca. 15 Å. Right: intervening peptide backbone between the donor and acceptor. Main chain H-bonds are shown dotted in yellow. Side chains and the two nonparticipating helices have been omitted for clarity. Graphics were produced using Molscript[43] and Raster3d.[44]

Reductive pulse radiolysis experiments were performed using the Brookhaven National Laboratory 2 MeV Van de Graaf generator using the aqueous electron as a reducing agent and using a PC-controlled, CAMAC-based control and data acquisition system.[30] Digitizer traces were fit to double first-order kinetics with the baseline offset by nonlinear least-squares methods. Experiments were performed in radiolysis buffer; sodium phosphate (10 mM, pH6), sodium perchlorate (50 mM), *tert*-butyl alcohol (100 mM). Samples were monitored at 380 nm to monitor the disappearance of the $[Ru(bpy)_2(bpy^-)]^+$ species and at 600 nm to observe the lifetime of the solvated electron.

Steady-state circular dichroism (CD) and chemical denaturation experiments were performed as previously described[26] and the data were analyzed using a two-state unfolding model with linear extrapolation to zero denaturant concentration.[31]

Results

Structure and Stability of the H-Bond Deletion Variants. The parent structure, $Ru(\alpha P)_2\alpha P9H$, and the H-bond deletion variants are all highly (and equally) helical in solution, as judged by the circular dichroism spectra. We conclude that deletion of a single H-bond does not lead to a substantial change in the time-averaged secondary structure of the three-helix bundle. As previously reported,[28] a single main chain hydrogen bond deletion *does* affect the global stability of the protein toward unfolding. Comparison of the chemical denaturation profiles of the parent construct with the three H-bond deletion variants (Table 1) indicates that the latter are less stable than the parent, with a similar change in free energy of unfolding associated with the H-bond deletion. The stability data carry two implications. First, the data suggest that the context dependence of main chain H-bond deletion is modest and is most pronounced when the H-bond deletion occurs at a position along the helix that is exposed to solvent. The values of $\Delta\Delta G_{unfolding} = 0.8 \pm 0.3$ kcal per H-bond compares well with values reported for main chain H-bond deletions in other studies.[28,32−36] Second, all the proteins remain more than 90% folded under the conditions of the electron-transfer experiments. Any differences observed in the experiments should reflect differences in electronic coupling associated with H-bond deletion rather than perturbations of ET rates due to an equilibrium population containing unfolded species.

TABLE 1: Unfolding Free Energies and Estimated H-Bond Solvent Exposure for the Three-Helix Bundles Used in This Study[a]

	$\Delta G°_{unfolding}$ (cal M^{-1})	$\Delta\Delta G°_{unfolding}$ (cal M^{-1})	% solvent accessibility
$Ru(\alpha P)_2\alpha P9H$	2450 (100)		
$Ru(\alpha P)_2\alpha P9H\varphi$(QH)	1350 (150)	1100 (200)	50
$Ru(\alpha P)_2\alpha P9H\varphi$ (LQ)	1850 (100)	600 (150)	10
$Ru(\alpha P)_2\alpha P9H\varphi$ (KL)	1750 (100)	700 (150)	20

[a] Unfolding curves were fit to a two state unfolding model with linear extrapolation to zero denaturant concentration. Solvent exposure of hydrogen bonds was estimated from molecular models.

Comparisons of Electron Transfer between "Wild Type" and H-Bond Deletion Variants. The electron transfer reactions were generally well behaved. Typical transient kinetics are shown in Figure 2a. The transients are biexponential with a fast phase and a slower phase. The slower phase can be assigned to the decay of unreacted material, which has no ruthenium pentammine acceptor. The faster phase comprises both the expected first-order component and a second-order component corresponding to intermolecular electron transfer. The first-order component is the sum of the intrinsic decay rate of the $[Ru(bpy)_2(bpy^-)]^+$ and decay due to intramolecular electron transfer.

The second-order component is best separated by studies of the concentration dependence of the reactions, as shown in Figure 2b. The resulting parameters suggest that the bimolecular

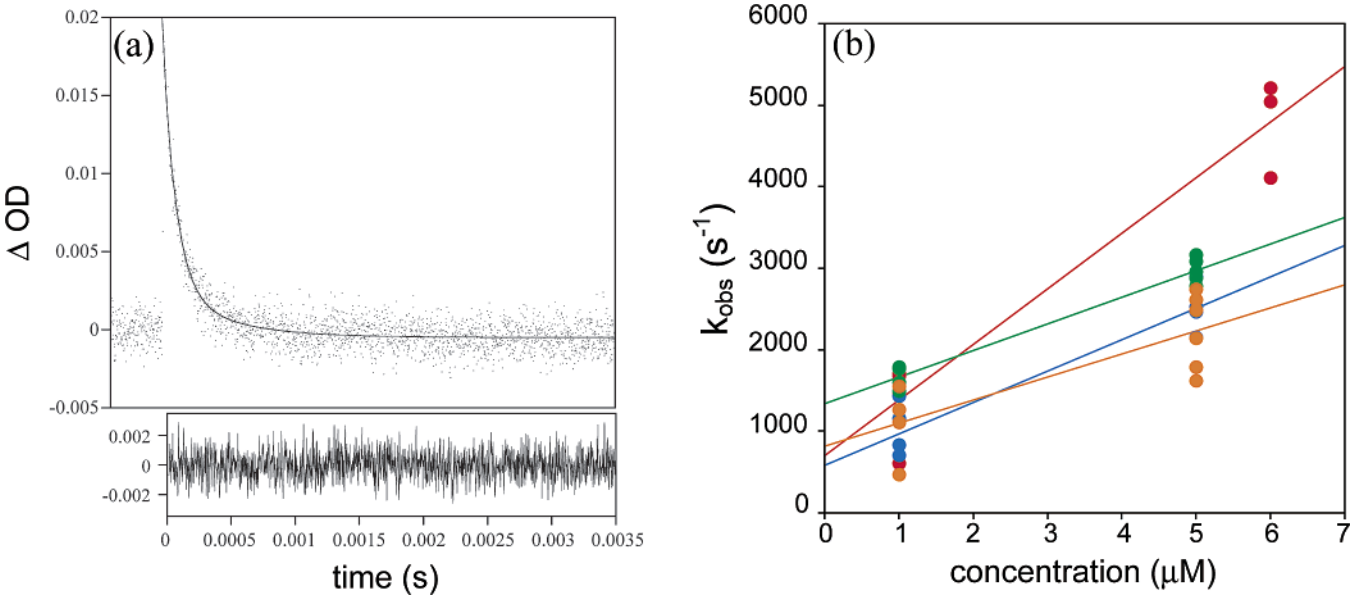

Figure 2. (a) Time dependence of absorbance at 380 nm in a typical pulse radiolysis experiment. The solid line is a fit to two exponentials and an offset. The residuals are shown below. (b) Concentration dependence of observed rates: (red) Ru(αP)$_2$αP9H; (blue) Ru(αP)$_2$αP9Hφ(QH); (green) Ru(αP)$_2$αP9Hφ(KL); (orange) Ru(αP)$_2\varphi$P9Hφ(LQ).

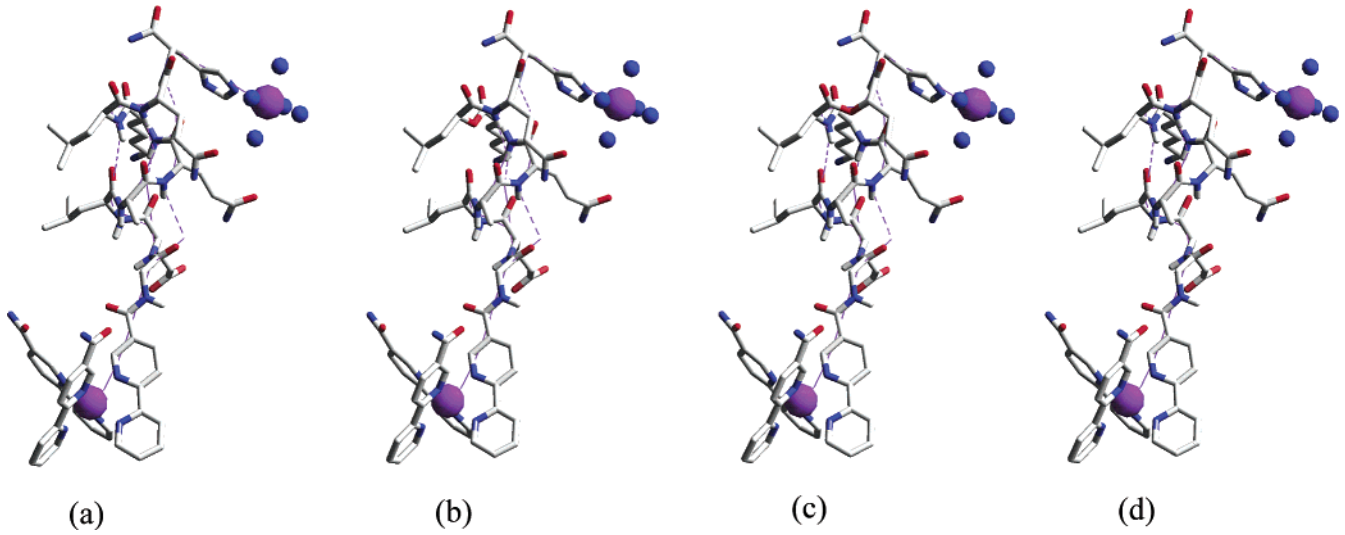

Figure 3. Greenpath calculated electron-transfer pathways and donor−acceptor coupling. (a) All H-bonds intact, 4 pathways predicted, 4.83 × 10^{-7} eV^2 total coupling. (b) φ(KL), 3 pathways predicted, 3.44 × 10^{-7} eV^2 total coupling. (c) φ(LQ), 3 pathways predicted, 3.74 × 10^{-7} eV^2 total coupling. (d) φ(QH), 2 pathways predicted, 2.48 × 10^{-7} eV^2 total coupling.

rate is near that allowed by diffusion control: $k_2 \approx 5 \pm 1 \times 10^8$ M^{-1} s^{-1}. Such a collisional process is not expected to be sensitive to details of internal hydrogen bonding. Consistent with this expectation, the bimolecular rate constants are the same within estimated experimental variance for all the derivatives. The intrinsic decay rates are obtained from the ordinate intercepts of the plot shown in Figure 2b (extrapolation to zero concentration). The intramolecular electron-transfer rates are then obtained from the ordinate intercepts less the intrinsic decay rate measured for Ru(αP)$_2$αP9H with no[Ru(NH$_3$)$_5$]$^{3+}$ acceptor. The electron-transfer rates for the four systems investigated are presented in Table 2.

TABLE 2: Unimolecular Electron Transfer Rates Determined from Pulse Radiolysis Experiments

	k_{obs} (s^{-1})	k_{int} (s^{-1})	$k_{et} = k_{obs} - k_{int}$
Ru(αP)2αP9H	900 (300)	200 (100)	700 (300)
Ru(αP)2αP9Hφ(QH)	800 (400)	200 (100)	600 (400)
Ru(αP)2αP9φ(LQ)	1500 (200)	200 (100)	1300 (200)
Ru(αP)$_2$αP9Hφ (KL)	1000 (500)	200 (100)	800 (500)

Discussion

Using a synthetic approach, we prepared four different helical peptides: the parent, or "wild type" structure with all H-bonds intact, and three homologues, each of which contains a single hydrogen bond deletion. In the first of these, Ru(αP)$_2$αP9Hφ(QH), the deletion is immediately adjacent to the redox site. For the second, Ru(αP)$_2$αP9Hφ(LQ), the deletion is one residue closer to the N-terminus of the helix, and in the third, Ru(αP)$_2$αP9Hφ(KL), it is two residues closer. The NMR structure of the homotrimeric complex [Co(αP5H)$_3$]$^{2+}$ was recently published[37] and reveals the expected α-helicity throughout the region probed by our deletion experiments.

The prediction of a pure "distance" model is that all the peptides (H-bond deleted or not) will react at the same rate, whereas network models predict a trend in reactivity wt > φ(KL) > φ(LQ) > φ(QH). Specifically, Dutton's "Golden Rule"

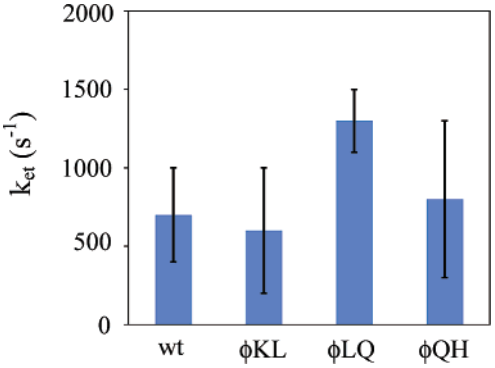

Figure 4. Electron-transfer rates for the four systems under investigation. Details of the calculation of ET rates and identities of the peptides are given in the text.

rates calculator[38] predicts an electron-transfer rate of 1380 s^{-1} for a Ru(II)−Ru(III) distance of 19 Å, a driving force of −1.2 eV and a reorganization energy of 0.8 eV. In contrast, the Green's function network analysis of "greenpath"[39] predicts the pathways shown in Figure 3. (In examining pathways, no sampling was done over accessible geometries of the complex. If flexible, the dominant pathways might change.)

Semiclassical theory gives the rate of electron-transfer k_{et} as

$$k_{et} = \left(\frac{4\pi^3}{h^2 \lambda k_B T}\right)^{1/2} H_{DA}{}^2 \exp\left(\frac{-(\Delta G^\circ + \lambda)^2}{4\lambda k_B T}\right)$$

The values of H^2 calculated above are directly proportional to the ET rates for the various species. Thus the electron transfer the rate in the "wild type" is predicted to be almost twice that of the φ(QH) variant.

Kinetic studies of electron transfer between the $[Ru(bpy)_3]^{2+}$ site and the $[Ru(NH_3)_5(his)]^{3+}$ site were carried out using pulse radiolysis, as previously described.[27,28,30] The data are summarized in Figure 4 and in Table 2.

Considering the experimental error, the data are most simply described by a model in which the rate does not depend on a specific hydrogen bonded pathway, for example a simple "distance" model. Given the exponential dependencies implicit in the model, the calculated rate is astonishingly close to those observed experimentally. Although a pathways model is not explicitly excluded, there is no clear implication of any of the deleted H-bonds in any of the calculated pathways. Indeed, analysis of the residuals returns a smaller estimated standard deviation (esd) over the entire data set compared to the average esd of the individual data sets. It should perhaps be noted that an all σ-bond pathway also predicts no change upon deletion of any H-bond; however, the total distance in this case (>40 Å) is such that the rates would be too slow to measure.

In summary, perturbation (or lack thereof) of ET rates by the deletion of hydrogen bonds from a synthetic protein backbone supports the notion that a packing density model[40] is identical to a pathway model in systems offering multiple pathways.[41,42]

Acknowledgment. We thank Drs. Dorothy Little and John Eng of Princeton University for their expertise with electrospray mass spectrometry. This work was supported by grant CHE-9729124 for which the National Science Foundation Division of Chemistry is gratefully acknowledged. The work performed at Brookhaven National Laboratory was funded under contract DE-AC02-98CH10886 with the U.S. Department of Energy and supported by its Division of Chemical Sciences, Office of Basic Energy Sciences.

Supporting Information Available: Experimental details of the synthesis of depsipeptides and their ruthenium complexes. This material is available free of charge via the Internet at http://pubs.acs.org.

References and Notes

(1) Gray, H. B.; Winkler, J. R. *Annu. Rev. Biochem.* **1996**, *65*, 537−561.
(2) Cukier, R. I.; Nocera, D. G. *Annu. Rev. Phys. Chem.* **1998**, *49*, 337−369.
(3) Bendall, D. S., Ed. *Protein Electron Transfer*; BIOS Scientific Publishers: Oxford, U.K., 1996.
(4) Marcus, R. A.; Sutin, N. *Biochim. Biophys. Acta* **1985**, *811*, 265−322.
(5) Moser, C. C.; Page, C. C.; Farid, R.; Dutton, P. L. J. *Bioenerg. Biomembr.* **1995**, *27*, 263−274.
(6) Moser, C. C.; Page, C. C.; Chen, X.; Dutton, P. L. *J. Biol. Inorg. Chem.* **1997**, *2*, 393−398.
(7) Williams, R. J. P. *J. Biol. Inorg. Chem.* **1997**, *2*, 373−377.
(8) Hopfield, J. J. *Proc. Natl. Acad. Sci. U.S.A.* **1974**, *71*, 3640−3644.
(9) Wuttke, D. S.; Bjerrum, M. J.; Winkler, J. R.; Gray, H. B. *Science* **1992**, *256*, 1007−1009.
(10) Onuchic, J. N.; Beratan, D. N.; Winkler, J. R.; Gray, H. B. *Annu. Rev. Biophys. Biomol. Struct.* **1992**, *21*, 349−377.
(11) Curry, W. B.; Grabe, M. D.; Kurnikov, I. V.; Skourtis, S. S.; Beratan, D. N.; Regan, J. J.; Aquino, A. J. A.; Beroza, P.; Onuchic, J. N. J. *Bioenerg. Biomembr.* **1995**, *27*, 285−293.
(12) Beratan, D. N.; Betts, J. N.; Onuchic, J. N. *Science* **1991**, *252*, 1285−1288.
(13) Skourtis, S. S.; Beratan, D. N. *J. Biol. Inorg. Chem.* **1997**, *2*, 378−386.
(14) Skourtis, S. S.; Beratan, D. N. *Adv. Chem. Phys.* **1997**, *106*, 377−452.
(15) Regan, J. J.; DiBiblio, A. J.; Langen, R.; Skov, L. K.; Winkler, J. R.; Gray, H. B.; Onuchic, J. N. *Chem. Biol.* **1995**, *2*, 489−496.
(16) Isied, S. S.; Ogawa, M. Y.; Wishart, J. F. *Chem. Rev.* **1992**, *92*, 381−394.
(17) Cabana, L. A.; Schanze, K. S. *Adv. Chem. Ser.* **1990**, *226*, 101−124.
(18) DeRege, P. J. F.; Williams, S. A.; Therien, M. J. *Science* **1995**, *269*, 1409−1413.
(19) Turro, C.; Chang, C. K.; Leroi, G. E.; Cukier, R. I.; Nocera, D. G. *J. Am. Chem. Soc.* **1992**, *114*, 4013−4015.
(20) Harriman, A.; Kubo, Y.; Sessler, J. L. *J. Am. Chem. Soc.* **1992**, *114*, 388−390.
(21) Williamson, D. A.; Bowler, B. E. *J. Am. Chem. Soc.* **1998**, *120*, 10902−10911.
(22) Kirby, J. P.; Roberts, J. A.; Nocera, D. G. *J. Am. Chem. Soc.* **1997**, *119*, 9230−9236.
(23) deRege, P. J. F.; Williams, S. A.; Therien, M. J. *Science* **1995**, *269*, 1409−1413.
(24) Ghadiri, M. R.; Soares, C.; Choi, C. *J. Am. Chem. Soc.* **1992**, *114*, 825−831.
(25) Ghadiri, M. R.; Case, M. A. *Angew. Chem., Int. Ed.* **1993**, *97*, 1669−1680.
(26) Case, M. A.; Ghadiri, M. R.; Mutz, M. W.; McLendon, G. L. *Chirality* **1998**, *10*, 35−40.
(27) Mutz, M. W.; Case, M. A.; Wishart, J. F.; Ghadiri, M. R.; McLendon, G. L. *J. Am. Chem. Soc.* **1999**, *121*, 858−859.
(28) Zhou, J.; Case, M. A.; Wishart, J. F.; McLendon, G. L. *J. Phys. Chem. B* **1998**, *102*, 9975−9980.
(29) Case, M. A.; McLendon, G. L. *J. Am. Chem. Soc.* **2000**, *122*, 8089−8090.
(30) Wishart, J. F.; Sun, J.; Cho, M.; Su, C.; Isied, S. S. *J. Phys. Chem. B* **1997**, *101*, 687−698.
(31) Pace, C. N. *Methods Enzymol.* **1986**, *131*, 267−280.
(32) Shin, I.; Ting, A. Y.; Schultz, P. G. *J. Am. Chem. Soc.* **1997**, *119*, 12667−12668.
(33) Koh, J. T.; Cornish, V. W.; Schultz, P. G. *Biochemistry* **1997**, *36*, 11314−11322.
(34) Chapman, E.; Thorson, J. S.; Schultz, P. G. *J. Am. Chem. Soc.* **1997**, *119*, 7151−7152.
(35) Isied, S. S. *Adv. Chem. Ser.* **1990**, *226*, 91−100.
(36) LaChance-Galang, K. J.; Doan, P. E.; Clarke, M. J.; Rao, U.; Yamano, A.; Hoffman, B. M. *J. Am. Chem. Soc.* **1995**, *117*, 3529−3538.

(37) Gochin, M.; Khorosheva, V.; Case, M. A. *J. Am. Chem. Soc.* **2002**, *124*, 11018−11028.

(38) http://www.uphs.upenn.edu/biocbiop/local_pages/dutton_lab.html.

(39) Regan, J. J. "greenpath software 0.95", Jeffrey J. Regan, San Diego, 1993.

(40) Page, C. C.; Moser, C. C.; Chen, X.; Dutton, P. L. *Nature*, **1999**, *402*, 47−52.

(41) Beratan, D. N.; Onuchic, J. N.; Betts, J. N.; Bowler, B. E.; Gray, H. B. *J. Am. Chem. Soc.* **1990**, *112*, 7915−7921.

(42) Jones, M. L.; Kurnikov, I. V.; Beratan, D. N. *J. Phys. Chem. A* **2002**, *106*, 2002−2006.

(43) Kraulis, P. J. *J. Appl. Crystallogr.* **1991**, *24*, 946−950.

(44) Merritt, E. A.; Bacon, D. J. *Methods Enzymol.* **1997**, *277*, 505−524.